*J. Fluid Mech.* (2012), *vol.* 698, *pp.* 73–92. © Cambridge University Press 2012 
doi:10.1017/jfm.2012.45

# Generalized two-dimensional Lagally theorem with free vortices and its application to fluid–body interaction problems

**C. T. Wu[1], F.-L. Yang[2]† and D. L. Young[1]†**

[1] Department of Civil Engineering, National Taiwan University, Taipei 10617, Taiwan

[2] Department of Mechanical Engineering, National Taiwan University, Taipei 10617, Taiwan

(Received 28 February 2011; revised 28 October 2011; accepted 21 January 2012;
first published online 16 March 2012)

The Lagally theorem describes the unsteady hydrodynamic force on a rigid body exhibiting arbitrary motion in an inviscid and incompressible fluid by the properties of the singularities employed to generate the flow and the body motion and to meet the boundary condition. So far, only sources and dipoles have been considered, and the present work extends the theorem to include free vortices in a two-dimensional flow. The present extension is validated by reproducing the system dynamics or the force evolution of three literature problems: (i) a free cylinder interacting with a free vortex; (ii) the moving Föppl problem; and (iii) a cylinder in constant normal approach to a fixed identical cylinder. This work further extends the bifurcation analysis on the moving Föppl problem by including the solid-to-liquid density ratio as a new parameter, in addition to the system total impulse and the vortex strength. We then apply the theorem to the problem where a moving Föppl system is made to approach a fixed or a free neutrally buoyant target cylinder of identical size from far away. The force developed on each cylinder is examined with respect to the vortex pair configuration and the target mobility. When approaching a fixed target, a greater force is developed if the vortex pair has stronger circulation and larger structure. The mobility of the target cylinder, however, can modify the hydrodynamic force by reducing its magnitude and reversing the force ordering with respect to the vortex pair configuration found for the case with fixed target. Possible mechanisms for such a change of force nature are given based on the currently derived equation of motion.

**Key words:** flow–structure interactions, general fluid mechanics, vortex interactions

## 1. Introduction

The interaction between rigid bodies and their ambient flow has been investigated extensively because of its common occurrence in engineering applications, industrial processes and natural hazards. When the effect of liquid viscosity is confined in flow regimes much smaller than the immersed bodies or the flow domain, the fluid motion can be approximated by a potential flow governed by the Laplace equation. The solution, which gives the potential function of the flow, can thus be constructed by superposing the fundamental solutions chosen specifically to generate the desired

† Email addresses for correspondence: fulingyang@ntu.edu.tw, dlyoung@ntu.edu.tw

https://doi.org/10.1017/jfm.2012.45 Published online by Cambridge University Press

motion and to meet the boundary condition. To estimate the hydrodynamic force and torque on the objects, the Blasius theorem can be employed, which considers the rate of change of fluid impulse. The resulting formulae are often expressed in terms of the flow potential function since its gradient gives the velocity field required when using the Bernoulli equation to derive the surface pressure distribution (Lamb 1932; Milne-Thompson 1968).

On this thread of research, Lagally (1922) developed a three-dimensional theorem that describes the quasi-steady hydrodynamic force and torque for an immersed object in terms of the strengths and positions of the singularities employed to generate specific flow fields. Lagally's work was extended later by Cummins (1953) to incorporate unsteady flow condition. These derivations were consolidated by Landweber & Yih (1956), who took an alternative but powerful approach to give the three-dimensional force and the torque expressions by employing only the singularities, isolated or distributed, *within* the body. The theorem for the case with deformable bodies in unsteady flow was considered by Landweber & Miloh (1980); a shorter and simpler derivation for a body in translation was given by Biesheuvel (1985). These authors also connected their results to the Taylor theorem, which represents the added mass tensor of an immersed translating object using the strengths and the locations of its internal singularities (Taylor 1928; Birkhoff 1950; Landweber 1956; Landweber & Yih 1956; Landweber & Chwang 1989). The advantage of using *internal* singularities is especially appreciated in problems with multiple objects when the hydrodynamic force on each individual body is of interest. Such information is not available from the conventional Lagally theorem, since it gives a *lumped sum* of the hydrodynamic forces from *all* the objects. So far, only dipoles and isolated or distributed sources have been considered, and the inclusion of two-dimensional free vortices, or vortex filaments in three-dimensional flows, has been neglected. Thus, the main purpose of this paper is to extend the two-dimensional Lagally theorem by considering free vortices, as a supplement to the work of Landweber & Yih (1956).

To validate the current extension, the generalized Lagally theorem has been applied to study the interaction of a free solid cylinder with single or paired free vortices of opposite strengths following the literature. In particular, the pair of free vortices of opposite strengths will be referred to as a *vortex pair* hereinafter. Eames, Landeryou & Flór (2007) studied such a problem under the condition of zero total flow impulse. Shashikanth *et al.* (2002) and Borisov, Mamaev & Ramodanov (2003) independently employed the Hamiltonian mechanics to derive the equation of motion for a cylinder that interacts with multiple free vortices. Shashikanth (2006) simplified the formulation for the problem when a vortex pair moves behind a neutrally buoyant cylinder. This problem is known as the classical moving Föppl problem, to which Shashikanth studied the vortex–cylinder interaction and possible system equilibrium configurations. All the reported dynamic equations and system dynamics can be reproduced with the current theorem. We further examine the system equilibrium configuration by considering different solid densities and vortex strengths.

We then continue to two-cylinder problems, limiting ourselves to the condition when one approaches constantly to the other of identical size and of liquid density. When the target is fixed, several theoretical analyses have been conducted to examine the hydrodynamic force developed on each cylinder on different frameworks. The work by Landweber & Shahshahan (1991) is derived in the framework of Lagrangian mechanics, which is further integrated with the generalized Taylor theorem (Landweber & Chwang 1989); Wang (2004) and Bampalas & Graham (2008) use the extended Blasius theorem (Milne-Thompson 1968); and Tchieu, Crowdy & Leonard

https://doi.org/10.1017/jfm.2012.45 Published online by Cambridge University Press

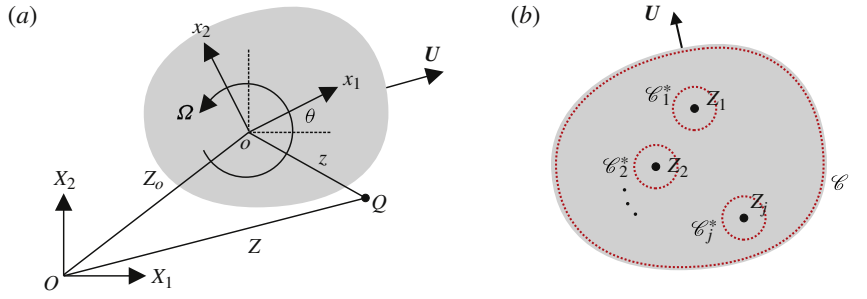



FIGURE 1. (Colour online available at journals.cambridge.org/flm) (*a*) Schematic diagram for a moving object in the inertial and the body-fixed reference frames, $OX_1X_2$ and $ox_1x_2$. The point of interest, $Q$, is at $z$ in $ox_1x_2$ but at $Z = Z_o + \mathrm{e}^{\mathrm{i}\theta}z$ in $OX_1X_2$. Here, $Z_o$ is the position of the moving reference frame in $OX_1X_2$ and $\theta$ is the angle between $OX_1$ and $ox_1$. (*b*) Illustration of the integration contour: on the object surface $\mathscr{C}$ or around the internal singularities, $\mathscr{C}_j^*$.

(2010) use a special conformal mapping to generate the potential function and numerical contour integration to obtain the force. The force evolution profiles obtained in this work agree with most of the literature results, except for Wang's data, the deviation from which will be discussed later.

This two-cylinder problem is extended in this work to include a vortex pair behind a cylinder in constant approach to a fixed or a free target cylinder. The vortex pair is assigned initially to the moving Föppl equilibrium configuration under the condition that the target cylinder is sufficiently far away that its perturbation on the adopted configuration is negligible. The force evolution profiles with or without the target mobility under various vortex pair configurations are compared to reveal how the hydrodynamic forces are developed in various flow conditions. It is worth noting that such a problem of two cylinders and multiple vortices may also be studied in the more versatile theoretical framework developed by Crowdy and his coworkers, who use the so-called Schottky–Klein prime function to construct the potential function (Crowdy & Marshall 2005*a*,*b*; Crowdy 2008, 2010). The major advantage of the current Lagally theorem, however, is that the force on each cylinder can be obtained by straightforward algebraic calculations using the strengths and locations of the system singularities.

The paper is organized as follows. The generalized Lagally theorem is developed in § 2 and problems with a single cylinder are examined in § 3. The equation of motion for a system with two cylinders exhibiting in-line motion with a vortex pair are then derived in § 4. We then continue to study how the hydrodynamic force develops on each cylinder when one approaches without or with a vortex pair. Finally, § 5 summarizes this work and comments on possible directions for future research.

## 2. Extension of the generalized Lagally theorem

The conventional two-dimensional Lagally theorem that considers sources and dipoles is revisited here in terms of complex variables to include free vortices, following the approach and the sign convention of Milne-Thompson (1968). Let a solid object move and rotate at $\boldsymbol{U}$ and $\boldsymbol{\Omega}$ relative to a fixed inertial reference frame $OX_1X_2$ in an unbounded inviscid and incompressible fluid at rest at infinity, as depicted in figure 1(*a*). A Cartesian coordinate system $ox_1x_2$ is fixed to a point $o$ on the body and its position relative to $OX_1X_2$ is $Z_o$. The positions of a point $Q$ in both reference

https://doi.org/10.1017/jfm.2012.45 Published online by Cambridge University Press

frames, $Z$ and $z$, are related by $Z = Z_o + \mathrm{e}^{\mathrm{i}\theta} z$, where $\theta$ is the angle between $OX_1$ and $ox_1$. In the following derivations, variables in the moving reference frame and any function in terms of the variables therein will be denoted with over-tilde.

The flow field, $\tilde{v} = \tilde{v}_1 + \mathrm{i}\tilde{v}_2$, is irrotational in $OX_1X_2$ and can be described by $\tilde{v} = -\overline{\mathrm{d}\tilde{w}/\mathrm{d}z}$, where the complex velocity potential, $\tilde{w} = \tilde{\phi} + \mathrm{i}\tilde{\psi}$, is composed of the potential and the stream functions, $\tilde{\phi}$ and $\tilde{\psi}$. The bar over a complex variable denotes its conjugate. The pressure equation in the moving frame can be expressed as

$$\frac{\tilde{p}}{\rho} + \frac{1}{2}q_r^2 - \frac{\partial\tilde{\phi}}{\partial t} - \frac{1}{2}(\tilde{U} + \mathrm{i}\Omega z)\,\overline{(\tilde{U} + \mathrm{i}\Omega z)} = E(t), \tag{2.1}$$

where $\tilde{p}$ is the pressure, $\rho$ is the constant fluid density, $q_r = |\tilde{v} - \tilde{U} - \mathrm{i}\Omega z|$ is the flow speed relative to $ox_1x_2$, and $E(t)$ is a time-dependent function. The hydrodynamic force exerted on the body can be calculated by integrating the hydrodynamic pressure distribution around the object contour, $\mathscr{C}$, as

$$\begin{aligned}\tilde{F} = &-\tfrac{1}{2}\mathrm{i}\rho\overline{\int_{\mathscr{C}}\left(\frac{\mathrm{d}\tilde{w}}{\mathrm{d}z}\right)^2\mathrm{d}z} + \rho\Omega\int_{\mathscr{C}} z\,\mathrm{d}\tilde{w} + \mathrm{i}\rho\int_{\mathscr{C}}\frac{\partial\tilde{w}}{\partial t}\,\mathrm{d}z\\ &+ \mathrm{i}m_d\Omega(\tilde{U} + \mathrm{i}\Omega\tilde{z}_c) + m_d\frac{\partial}{\partial t}(\tilde{U} + \mathrm{i}\Omega\tilde{z}_c),\end{aligned} \tag{2.2}$$

where $\tilde{z}_c$ is the centroid of the body and $m_d$ is the mass of fluid displaced by the body. This force formula is known as the extended Blasius theorem and can be reduced to the conventional Blasius theorem, i.e. the first term on the right-hand side of (2.2), when the object is fixed in space and the flow is steady (Milne-Thompson 1968). Now, we proceed to derive the generalized Lagally theorem with free vortices.

Through integration by parts, the quantity in the second term on the right-hand side of (2.2) becomes $\int_{\mathscr{C}} z\,\mathrm{d}\tilde{w} = z\tilde{w}|_{\mathscr{C}} - \int_{\mathscr{C}}\tilde{w}\,\mathrm{d}z$, which may be simplified by the properties of *internal* singularities. These singularities are either images imposed to satisfy the no-penetration boundary condition or those adopted to generate an object motion. We first consider $N$ *image* sources and $M$ *image* vortices at $z_j^s$ and $z_j^v$ within $\mathscr{C}$ whose complex potential functions are $\tilde{w}_j^s(z) = -m_j\ln(z - z_j^s)$ and $\tilde{w}_j^v(z) = \mathrm{i}\kappa_j\ln(z - z_j^v)$, where $m_j$ and $\kappa_j$ are individual singularity strengths. If $z_a$ is a branch cut point on $\mathscr{C}$, one internal source contributes $-2\pi\mathrm{i}m_jz_a$ to $z\tilde{w}|_{\mathscr{C}}$ because its potential is multi-valued. Adopting the same branch cut point, an internal image vortex generates $-2\pi\kappa_jz_a$. Note here that if a different branch point is employed, the same result can still be obtained. Thus, $z\tilde{w}|_{\mathscr{C}} = -2\pi z_a\left(\mathrm{i}\sum_{j=1}^N m_j + \sum_{j=1}^M\kappa_j\right)$ in which $\sum_{j=1}^N m_j = 0$ for mass conservation. Further, $\sum_{j=1}^M\kappa_j = 0$ since an external free vortex always generates a pair of image vortices of opposite signs within $\mathscr{C}$. Note that $z\tilde{w}|_{\mathscr{C}}$ vanishes for any internal dipole of strength $\mu_j$ at $z_j^d$ since $z\tilde{w}_j^d$, with $\tilde{w}_j^d(z) = \mu_j/(z - z_j^d)$, is single-valued around $\mathscr{C}$. Note that the present conclusion that $zw|_{\mathscr{C}} = 0$ no longer holds when internal sources or vortices are employed to create particular object dynamics, such as volume or shape change not considered in the current study. Further, when an external vortex is shed from the object, a bounded vortex of opposite sign should be generated within $\mathscr{C}$ in addition to the aforementioned image vortices (Saffman 1992). The object thus possesses circulation, and this scenario is also excluded in this work.

https://doi.org/10.1017/jfm.2012.45 Published online by Cambridge University Press

To obtain a force formula in $OX_1X_2$, the rate of change of a vector in $ox_1x_2$, $\tilde{\xi}$, can be converted into that in $OX_1X_2$ using $\dot{\xi}\mathrm{e}^{-\mathrm{i}\theta} = \mathrm{i}\Omega\tilde{\xi} + \dot{\tilde{\xi}}$, where the over-dot denotes the time derivative. Thus, the component $-\Omega\int_{\mathscr{C}}\tilde{w}\,\mathrm{d}z$ left in the second term on the right-hand side of (2.2) can be combined with the third term to give $\mathrm{i}\mathrm{e}^{-\mathrm{i}\theta}\,\mathrm{d}\left(\int_{\mathscr{C}} w\,\mathrm{d}Z\right)/\mathrm{d}t$ with $w(Z) = \tilde{w}(z(Z))$. Similarly, the last two terms involving $\tilde{U} + \mathrm{i}\Omega\tilde{z}_c$ can be grouped together. A general force formula in $OX_1X_2$ is obtained, agreeing with that found by Sedov (1965), as

$$F = -\tfrac{1}{2}\mathrm{i}\rho\overline{\int_{\mathscr{C}}\left(\frac{\mathrm{d}w}{\mathrm{d}Z}\right)^2\mathrm{d}Z} + \mathrm{i}\rho\frac{\mathrm{d}}{\mathrm{d}t}\int_{\mathscr{C}} w\,\mathrm{d}Z + m_d\frac{\mathrm{d}}{\mathrm{d}t}[U + \mathrm{i}\Omega(Z_c - Z_o)], \tag{2.3}$$

where $Z_c$ is the body centroid position in $OX_1X_2$.

Next, the complex velocity potential is decomposed into

$$w = \sum_{\alpha=1}^{3} U_\alpha w_\alpha + w_{ext} + w_{int}. \tag{2.4}$$

Here, the first term on the right-hand side is due to body translation, $(U_1, U_2)$, and rotation, $U_3 = \Omega$, with corresponding *normalized* potentials, $w_\alpha$ (Landweber & Yih 1956). The second term denotes functions with singularities exterior to $\mathscr{C}$ employed to represent specific ambient flow structures or motions of other coexisting bodies. The last term represents internal potential functions adopted with respect to the external singularities to ensure a no-penetration boundary condition on $\mathscr{C}$. With such a decomposition, the second term on the right-hand side of (2.3) becomes

$$\mathrm{i}\rho\frac{\mathrm{d}}{\mathrm{d}t}\int_{\mathscr{C}} w\,\mathrm{d}Z = \mathrm{i}\rho\sum_{\alpha=1}^{3}\frac{\mathrm{d}}{\mathrm{d}t}\left(U_\alpha\int_{\mathscr{C}} w_\alpha\,\mathrm{d}Z\right) + \mathrm{i}\rho\frac{\mathrm{d}}{\mathrm{d}t}\int_{\mathscr{C}} w_{int}\,\mathrm{d}Z, \tag{2.5}$$

in which $\int_{\mathscr{C}} w_{ext}\,\mathrm{d}Z = 0$ by Cauchy's integral theorem, since $w_{ext}$ is analytic within $\mathscr{C}$. The first term on the right-hand side of (2.5) can be further manipulated, following Landweber & Yih (1956), into $\mathrm{i}\rho\int_{\mathscr{C}} w_\alpha\,\mathrm{d}Z = \mathrm{i}\rho\int_{\mathscr{C}}\phi_\alpha\,\mathrm{d}Z - \rho\int_{\mathscr{C}}\psi_\alpha\,\mathrm{d}Z$, where the first term gives the conventional *added mass tensor*, following their notation, as

$$-\mathrm{i}\rho\int_{\mathscr{C}}\phi_\alpha\,\mathrm{d}Z = A_{\alpha1} + \mathrm{i}A_{\alpha2}. \tag{2.6}$$

In general, the added mass tensor is of full rank ($3\times3$ for a two-dimensional problem) and can be expressed in terms of the strengths and positions of the normalized potentials, $w_\alpha$, in (2.4). The added mass coefficients in the tensor can change in time with the object orientation or with the relative configuration with respect to other coexisting objects (Landweber & Chwang 1989; Yang 2010).

The integration of the stream function can proceed using integration by parts to give $-\rho\int_{\mathscr{C}} Zn_\alpha\,\mathrm{d}s$, with $(n_1, n_2)$ denoting the outward surface normal and $n_3 = (X_1 - X_{o1})n_2 - (X_2 - X_{o2})n_1$. This quantity is expressed by Landweber & Yih (1956) as another symmetric coefficient tensor, $-B_{\alpha j}$, as

$$B_{11} = B_{22} = m_d, \quad B_{21} = 0, \quad B_{31} = -m_d(X_{c2} - X_{o2}) \quad \text{and} \quad B_{32} = m_d(X_{c1} - X_{o1}). \tag{2.7}$$

Note that $B_{33}$ cannot be derived with the current formulation and has not been treated in all the cited references. With these coefficients, the term in parentheses on the right-hand side of (2.5) can be written as $U_\alpha[A_{\alpha1} + B_{\alpha1} + \mathrm{i}(A_{\alpha2} + B_{\alpha2})]$. Straightforward

https://doi.org/10.1017/jfm.2012.45 Published online by Cambridge University Press

manipulations follow to give $-\sum_{\alpha=1}^{3} U_\alpha(B_{\alpha 1} + \mathrm{i}B_{\alpha 2}) = -m_d[U + \mathrm{i}\Omega(Z_c - Z_o)]$ whose time derivative cancels the last term of (2.3) to give

$$F = -\tfrac{1}{2}\mathrm{i}\rho \overline{\int_{\mathscr{C}} \left(\frac{\mathrm{d}w}{\mathrm{d}Z}\right)^2 \mathrm{d}Z} - \sum_{\alpha=1}^{3} \frac{\mathrm{d}}{\mathrm{d}t}[U_\alpha(A_{\alpha 1} + \mathrm{i}A_{\alpha 2})] + \mathrm{i}\rho \frac{\mathrm{d}}{\mathrm{d}t} \int_{\mathscr{C}} w_{int}\, \mathrm{d}z. \tag{2.8}$$

The first term on the right-hand side of (2.8) is dynamically equivalent to the quasi-steady force in the classical Blasius force formula. The second term can generate the added mass force, $A_{\alpha j}\,\mathrm{d}U_\alpha/\mathrm{d}t$, for unsteady object motion but remains non-zero for a steady object due to $U_\alpha\,\mathrm{d}A_{\alpha j}/\mathrm{d}t$. This latter force component arises as a result of changes in object relative configuration. The last term of (2.8) accounts for the temporal variations of the strengths and positions of the internal image singularities. By transforming the line integral along $\mathscr{C}$ onto circles, $\mathscr{C}_1^*$, $\mathscr{C}_2^*$, ... and $\mathscr{C}_j^*$, centred at each internal singularity (see figure 1*b*), the integrals in (2.8) can be evaluated by the residue theorem. The final force formula in $OX_1X_2$ is found, in terms of the property of each *internal* singularity, as

$$F = -2\pi\rho \sum_{j\ all} \overline{\left(\mu_j \left.\frac{\mathrm{d}f_j}{\mathrm{d}Z}\right|_{Z_j^d} + m_j f_j|_{Z_j^s} - \mathrm{i}\kappa_j f_j|_{Z_j^v}\right)}$$
$$- \frac{\mathrm{d}}{\mathrm{d}t} \sum_{\alpha=1}^{3} [U_\alpha(A_{\alpha 1} + \mathrm{i}A_{\alpha 2})] - 2\pi\rho \frac{\mathrm{d}}{\mathrm{d}t} \sum_{j\ img} (\mu_j + m_j Z_j^s - \mathrm{i}\kappa_j Z_j^v). \tag{2.9}$$

The function $f_j = -\mathrm{d}(w - w_j)/\mathrm{d}Z$ in the first summation is the flow velocity induced by all the other singularities at an internal singularity location $Z_j$. Thus, each $f_j$ is different and will be referred to as the *partial velocity function* hereinafter. Note that the first summation in (2.9) is executed on *all* the singularities *within* $\mathscr{C}$ but the last group contains *only* the contributions of the internal *image* singularities, specially marked by *img* beneath the summation sign. The singularities employed to generate the body motion are not considered in the last summation since their effects have been accounted for in the second term. In comparison to the conventional Lagally theorem, which gives force in three dimensions (Lagally 1922; Cummins 1953; Landweber & Yih 1956; Biesheuvel 1985), (2.9) is two-dimensional and new force components due to free vortices are found.

## 3. Problems with one cylinder

In this section, (2.9) is first applied to derive the equation of motion for a single cylinder interacting with $N_v$ free vortices and applied to two literature problems to validate our force formula.

### 3.1. *Equations of motion*

Consider a non-rotating cylinder of radius $a$ and density $\rho_s$ moving at velocity $U = U_1 + \mathrm{i}U_2$ with $N_v$ free vortices of strengths $\kappa_j$ at $Z_j^v$. The resulting complex potential can be expressed following (2.4) as

$$w(Z) = \left(U_1 \frac{\mu_1}{Z - Z^c} + U_2 \frac{\mu_2}{Z - Z^c}\right) + \mathrm{i}\sum_{j=1}^{N_v} \kappa_j \ln(Z - Z_j^v) + \mathrm{i}\sum_{j=1}^{N_v} \kappa_j \ln\left(\frac{Z - Z^c}{Z - \hat{Z}_j^v}\right). \tag{3.1}$$

https://doi.org/10.1017/jfm.2012.45 Published online by Cambridge University Press

In (3.1), two dipoles of strengths $\mu_1 = a^2$ and $\mu_2 = \mathrm{i}a^2$ are employed at the cylinder centre $Z^c$ to represent the object motion along $OX_1$ and $OX_2$, respectively. To counterbalance the flux generated by the $N_v$ exterior free vortices, $2N_v$ internal image vortices of strengths $-\kappa_j$ and $\kappa_j$ at $\hat{Z}_j^v$ and $Z^c$ are used. Here $\hat{Z}_j^v = Z^c + (a^2/l_j^2)(Z_j^v - Z^c)$, with $l_j = |Z_j^v - Z^c|$, is the inverse point of $Z_j^v$ with respect to $\mathscr{C}$. The non-zero added mass coefficients for a circular cylinder are $A_{11} = A_{22} = \rho\pi a^2$, which remain constant since no other solid objects are present. Substituting the singularity strengths and positions into (2.9), an explicit force formula can be obtained to derive the equation of motion for the cylinder as

$$\rho_s \pi a^2 \frac{\mathrm{d}U}{\mathrm{d}t} = -2\pi\rho \overline{\left[ U_1\mu_1 \frac{\mathrm{d}f}{\mathrm{d}Z}\bigg|_{Z^c} + U_2\mu_2 \frac{\mathrm{d}f}{\mathrm{d}Z}\bigg|_{Z^c} + \mathrm{i}\sum_{j=1}^{N_v} \left( \kappa_j f\big|_{Z^c} - \kappa_j f\big|_{\hat{Z}_j^v} \right) \right]}$$
$$- \rho\pi a^2 \frac{\mathrm{d}U}{\mathrm{d}t} + \mathrm{i}2\pi\rho \frac{\mathrm{d}}{\mathrm{d}t} \sum_{j=1}^{N_v} \kappa_j (Z^c - \hat{Z}_j^v). \tag{3.2}$$

The partial velocity function is $f = -\mathrm{i}\sum_{j=1}^{N_v} \kappa_j/(Z - Z_j^v)$, which should vary for each singularity. However, it can be shown that the contributions from any pair of interior singularities, such as those employed in this problem, cancel out and only the contributions from the external vortices remain, and thus each $f$ is identical here.

Each free vortex moves at the flow velocity induced by *all* the other singularities at $Z_k^v$ as

$$\overline{\frac{\mathrm{d}Z_k^v}{\mathrm{d}t}} = \left[ \frac{U_1\mu_1}{(Z_k^v - Z^c)^2} + \frac{U_2\mu_2}{(Z_k^v - Z^c)^2} \right]$$
$$- \sum_{\substack{j=1 \\ j\neq k}}^{N_v} \frac{\mathrm{i}\kappa_j}{Z_k^v - Z_j^v} - \sum_{j=1}^{N_v} \mathrm{i}\kappa_j \left( \frac{1}{Z_k^v - Z^c} - \frac{1}{Z_k^v - \hat{Z}_j^v} \right), \tag{3.3}$$

for $k = 1, \ldots, N_v$. We then use (3.3) to simplify the first group on the right-hand side of (3.2) to obtain $\mathrm{i}2\pi\rho\, \mathrm{d}\left(\sum_{j=1}^{N_v} \kappa_j Z_j^v\right)/\mathrm{d}t$. Finally, when there is no external force applied on the cylinder–vortex system, (3.2) can be integrated in time to give

$$\rho_s \pi a^2 \frac{\mathrm{d}Z^c}{\mathrm{d}t} + \rho\pi a^2 \frac{\mathrm{d}Z^c}{\mathrm{d}t} - \mathrm{i}2\pi\rho \sum_{j=1}^{N_v} \kappa_j Z_j^v - \mathrm{i}2\pi\rho \sum_{j=1}^{N_v} \kappa_j (Z^c - \hat{Z}_j^v) = L_0, \tag{3.4}$$

with an integration constant, $L_0$, representing the conserved system total momentum. The first term is the object momentum and the following three terms are the fluid impulses generated by the unsteady object motion, the external free vortices and the internal image vortices, respectively.

### 3.2. *With one free vortex*

The first problem considers the interplay of a solid cylinder free to move in response to a free vortex of strength $\kappa$. The system behaviour has been investigated theoretically by Eames *et al.* (2007), where the equations of motion for both the cylinder and the free vortex are given explicitly after contour integration of the conventional Blasius theorem. With the current generalized Lagally theorem, identical formula describing

https://doi.org/10.1017/jfm.2012.45 Published online by Cambridge University Press

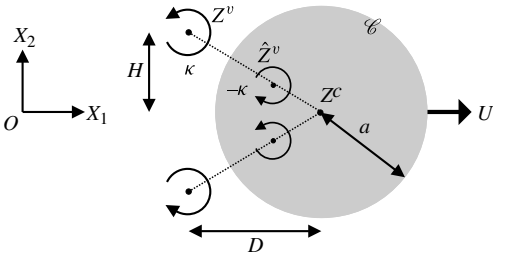



FIGURE 2. Schematic of the moving Föppl problem and the relevant variables.

the relative motion can be obtained from (3.4) using $N_v = 1$, $\kappa_1 = \kappa$ and $L_0 = 0$ as

$$\frac{\mathrm{d}Z^c}{\mathrm{d}t} = \frac{\mathrm{i}\Gamma}{\pi a^2(\rho_s/\rho + 1)}\left[Z_1^v - \frac{a^2}{l_1^2}(Z_1^v - Z^c)\right], \tag{3.5}$$

where $\Gamma = 2\pi\kappa$ is the circulation of the free vortex. Hence, the evolution trajectories for the point vortex and the cylinder presented in the figure 1 of their work can be exactly reproduced.

### 3.3. *With a vortex pair: the moving Föppl problem*

Next, we consider the moving Föppl problem, where a pair of vortices of opposite strengths, $\kappa_1 = -\kappa_2 = \kappa$, move behind a non-rotating cylinder of radius $a$ and density $\rho_s$ along $OX_1$ at velocity $U$, as depicted in figure 2. This vortex pair is in a symmetric configuration with respect to $OX_1$ with a half-span of $H$ and a horizontal distance $D$ from $Z^c$. The complementary set-up where a uniform flow passes a fixed cylinder with a downstream vortex pair is the classic Föppl problem, well examined in the literature (Föppl 1913; Milne-Thompson 1968; Marshall 2001). The moving Föppl problem appears in a few recent works that treat it as a perturbation problem, as introduced below.

Firstly, Shashikanth *et al.* (2002) develop a model for the interaction between a *neutrally buoyant* cylinder and $N$ free vortices in a potential flow using the Hamiltonian mechanics. Later, Shashikanth (2006) considers the case with only a unit vortex pair and evaluates how the *system total momentum*, $L_0$, modifies the equilibrium configuration of the vortex pair and the cylinder based on their relative motion. We extend the analysis by considering how the *solid-to-fluid density ratio*, $\gamma = \rho_s/\rho$, and the *vortex strength*, $\kappa$, alter the system equilibrium configuration. Here, we only probe the relative motion between the top vortex and the moving cylinder.

The equation of motion for the cylinder can be readily obtained by substituting $\kappa_1 = -\kappa_2 = \kappa$ and $Z_1^v = \overline{Z_2^v} = Z^v$ into (3.4) as

$$\rho\pi a^2(1+\gamma)\frac{\mathrm{d}Z^c}{\mathrm{d}t} - \mathrm{i}2\pi\rho\kappa\left(Z^v - \overline{Z^v} - \hat{Z}^v + \overline{\hat{Z}^v}\right) = L_0, \tag{3.6}$$

where $\hat{Z}^v = Z^c + (a^2/l^2)(Z^v - Z^c)$ with $l = |Z^v - Z^c|$. Note that, since the exterior vortices have opposite strengths, their image vortices at the cylinder centre mutually cancel out upon superposition. The top vortex moves with the flow velocity induced at $Z^v$ by all the other singularities as

$$\overline{\frac{\mathrm{d}Z^v}{\mathrm{d}t}} = \frac{Ua^2}{(Z^v - Z^c)^2} + \frac{\mathrm{i}\kappa}{Z^v - \overline{Z^v}} + \frac{\mathrm{i}\kappa}{Z^v - \hat{Z}^v} - \frac{\mathrm{i}\kappa}{Z^v - \overline{\hat{Z}^v}}. \tag{3.7}$$

https://doi.org/10.1017/jfm.2012.45 Published online by Cambridge University Press

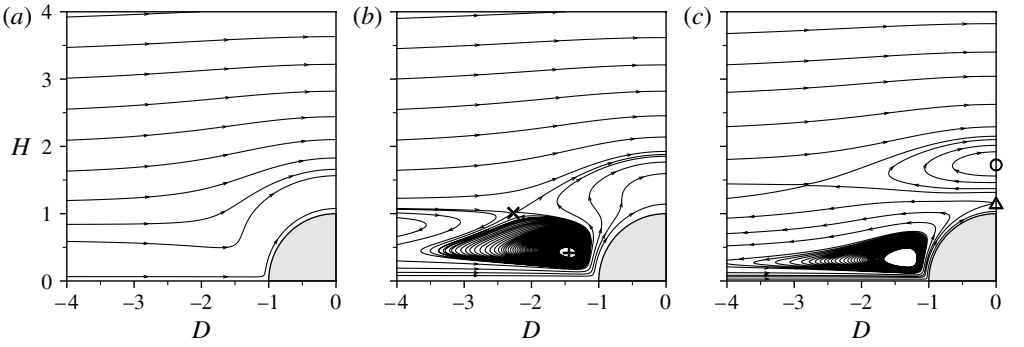



FIGURE 3. The trajectory of the top vortex relative to the moving cylinder in a moving Föppl system on the upstream side of the cylinder with $\gamma = 1.5$, $\kappa = 1.5$ and various $L_0$: (*a*) $L_0 = 5.0$; (*b*) $L_0 = 7.0$; (*c*) $L_0 = 9.0$. Föppl saddle and centre equilibrium points are marked by $\times$ and $+$ in panel (*b*). The symbols $\triangle$ and $\bigcirc$ in panel (*c*) denote the normal line saddle and centre equilibrium points.

Let $z^v = Z^v - Z^c = -D + \mathrm{i}H$. The relative motion between the top vortex and the cylinder can be obtained, using (3.6) and (3.7), as

$$\frac{\mathrm{d}z^v}{\mathrm{d}t} = \left(\frac{-4\kappa H}{1+\gamma}\,\frac{l^2-a^2}{l^2} + \frac{L_0}{(1+\gamma)\rho\pi}\right)\left(\frac{D^2 - 2\mathrm{i}DH - H^2}{l^4} - \frac{1}{a^2}\right) + \frac{\kappa}{2H} + \frac{\kappa(\mathrm{i}D + H)}{l^2 - a^2} + \frac{\kappa[-\mathrm{i}(l^2-a^2)D - (l^2+a^2)H]}{l^4 - 2a^2(D^2+H^2) + a^4}. \tag{3.8}$$

The influences of $L_0$, $\gamma$, $\kappa$ and the vortex pair structure, $D$ and $H$, are clearly revealed. This equation can be non-dimensionalized by $(D^*, H^*) = (D, H)/a$, $t^* = tU_0/a$, $\kappa^* = \kappa/(U_0 a)$ and $L_0^* = L_0/(\rho\pi a^2 U_0)$, where $U_0$ is the characteristic cylinder velocity. Omitting the asterisks, the real and imaginary parts of (3.8) describe how the vortex pair structure evolves in time with respect to $Z^c$ as

$$\frac{\mathrm{d}D}{\mathrm{d}t} = \left(\frac{-4\kappa H}{1+\gamma}\,\frac{l^2-1}{l^2} + \frac{L_0}{1+\gamma}\right)\left(1 - \frac{D^2 - H^2}{l^4}\right) - \frac{\kappa}{2H} - \frac{\kappa H}{l^2-1} + \frac{\kappa(l^2+1)H}{l^4 - 2(D^2-H^2) + 1}, \tag{3.9a}$$

$$\frac{\mathrm{d}H}{\mathrm{d}t} = -D\left[\left(\frac{-4\kappa H}{1+\gamma}\,\frac{l^2-1}{l^2} + \frac{L_0}{1+\gamma}\right)\frac{2H}{l^4} - \frac{\kappa}{l^2-1} + \frac{\kappa(l^2-1)}{l^4 - 2(D^2-H^2) + 1}\right]. \tag{3.9b}$$

Using $\gamma = 1$ and $\kappa = 1$, the equations given by Shashikanth (2006) can be readily obtained and the top vortex trajectory depicted for various $L_0$ in the cited work (figure 4 therein) can be exactly reproduced, further validating the current formulation.

Now, (3.9) is employed to investigate how the vortex–cylinder interaction changes with respect to $L_0$, $\gamma$ and $\kappa$ by examining the relative trajectory. Figure 3(*a–c*) shows the results on the upstream side of the cylinder for $\gamma = 1.5$, $\kappa = 1.5$ and three $L_0 = 5.0$, 7.0 and 9.0. In figure 3(*a*), the vortex always passes by the cylinder and no equilibrium point can be detected. With a greater $L_0$, two equilibrium configurations develop: an unstable *moving Föppl saddle* and a stable *centre* are marked by the cross ($\times$) and the plus ($+$) signs in figure 3(*b*), respectively. When $L_0$ is further increased to 9.0, two more equilibrium configurations appear along the line of $D = 0$. Following

https://doi.org/10.1017/jfm.2012.45 Published online by Cambridge University Press

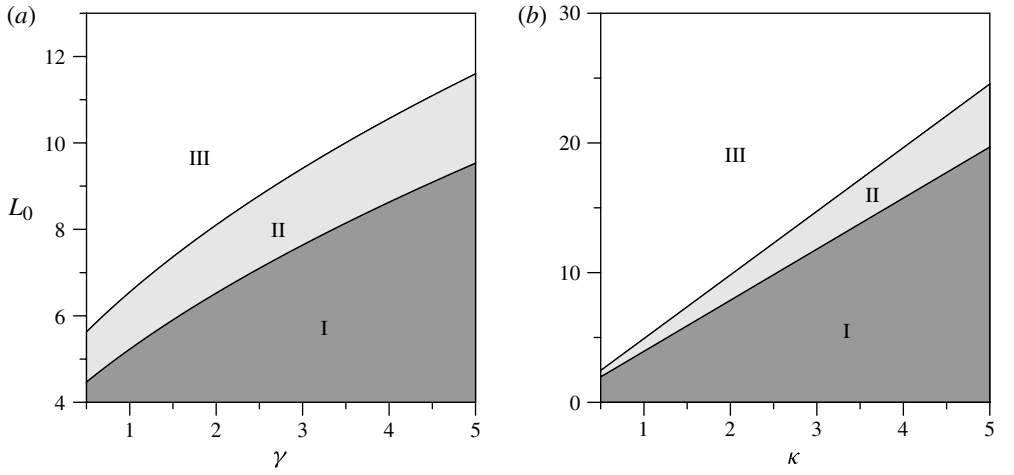



FIGURE 4. Equilibrium configuration for a moving Föppl system examined with respect to the three controlling parameters, i.e. system total momentum ($L_0$), solid-to-liquid density ratio ($\gamma$) and vortex strength ($\kappa$): (*a*) $\kappa = 1.5$; (*b*) $\gamma = 1.5$. The typical vortex trajectory developed in regimes I–III are illustrated in figure 3(*a–c*), respectively.

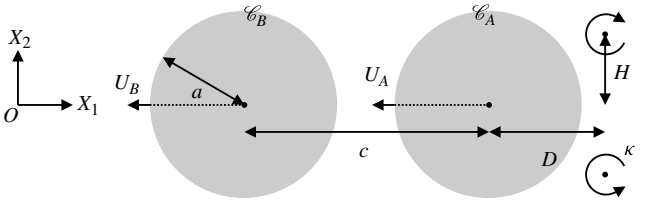



FIGURE 5. Schematic diagram of the problem where a moving Föppl system led by cylinder $\mathscr{C}_A$ is made to move at $U_A = -1$ towards a target cylinder $\mathscr{C}_B$ that is either fixed or free to move at an induced $U_B$. The vortex structure is denoted by $H$ and $D$ with respect to the location of $\mathscr{C}_A$.

Shashikanth (2006), the lower and the upper ones are referred to as the *moving normal line saddle* (△) and *centre* (◯), respectively, as marked in figure 3(*c*).

To fully understand how the system parameters $L_0$, $\gamma$ and $\kappa$ may control the equilibrium configuration, two bifurcation plots were generated in figures 4(*a*) and 4(*b*) with either $\kappa$ or $\gamma$ kept constant. On both plots, regimes I, II and III indicate the situation when no, two or four equilibrium points can be developed, like the cases portrayed in figure 3(*a–c*), respectively. Note that Eames *et al.* (2007) also studied the influence of $\gamma$ on the vortex–cylinder interaction in this system with unit $\kappa$ and zero $L_0$. Their equation of motion can also be reconstructed exactly by setting $\kappa = 1$ and $L_0 = 0$ in (3.9).

## 4. Application: problems of two identical cylinders with in-line motion

### 4.1. *Problem set-up and the governing equation*

To demonstrate how the current Lagally theorem may be exploited to study more complex problems, a second cylinder of identical size, $\mathscr{C}_B$, is introduced downstream of a moving Föppl system. The schematic diagram is provided in figure 5, where $\mathscr{C}_A$

https://doi.org/10.1017/jfm.2012.45 Published online by Cambridge University Press

with a vortex pair behind it is made to move at $U_A$ towards $\mathscr{C}_B$, which may be fixed or move at $U_B$. Let $Z^A$ and $Z^B$ denote the positions of the cylinder centres and $c = |Z^A - Z^B|$ be the inter-cylinder distance. The bottom and top free vortices behind $\mathscr{C}_A$ are of strengths $\kappa$ and $-\kappa$ and are located at $Z_o^{v+} = Z^A + D - \mathrm{i}H$ and $Z_o^{v-} = Z^A + D + \mathrm{i}H$.

The complex potential can be expressed, following (2.4), as $w(Z) = U_A w_A + U_B w_B + [\mathrm{i}\kappa \ln(Z - Z_o^{v+}) + w_{int}^{v+}] + [-\mathrm{i}\kappa \ln(Z - Z_o^{v-}) + w_{int}^{v-}]$, with $w_A$ or $w_B$ being the complex potential when $\mathscr{C}_A$ or $\mathscr{C}_B$ moves at unit velocity with the other held fixed and without any vortex. The two logarithmic functions in the brackets are the complex potentials for the bottom and the top free vortices, and $w_{int}^{v+}$ and $w_{int}^{v-}$ are the respective image systems. Here, $w_A$ is composed of two infinite series of dipoles in each cylinder led by the primary dipole of strength $\mu_0^A = a^2$ at $Z^A$ that represents the unit motion of $\mathscr{C}_A$. The strengths and locations of the successive images, $\mu_j^A$ and $Z_j^{dA}$, can be obtained, following Yang (2010), as

$$\mu_j^A = (-1)^j \left( \frac{\alpha - \beta}{\alpha^{j+1} - \beta^{j+1}} \right)^2 \mu_0^A \quad \text{for } j = 1, 2, 3 \ldots, \tag{4.1}$$

and

$$Z_j^{dA} = \begin{cases} Z^A - a\dfrac{\alpha^j - \beta^j}{\alpha^{j+1} - \beta^{j+1}} & \text{for } j = 0, 2, 4, \ldots \text{ in } \mathscr{C}_A, \\ Z^B + a\dfrac{\alpha^j - \beta^j}{\alpha^{j+1} - \beta^{j+1}} & \text{for } j = 1, 3, 5, \ldots \text{ in } \mathscr{C}_B, \end{cases} \tag{4.2}$$

with $\alpha, \beta = \left( c^* \pm \sqrt{c^{*2} - 4} \right)/2$ and $c^* = c/a$. Since $\mathscr{C}_B$ is of identical size to $\mathscr{C}_A$, $w_B$ can be formulated similarly, and both image systems possess the same dipole strength, giving $\mu_j^A = \mu_j^B = \mu_j$.

As for the vortex image system, we show the components in $w_{int}^{v+}$ which function counterbalances the flux generated by the bottom free vortex on $\mathscr{C}_A$ and $\mathscr{C}_B$. The first image in $\mathscr{C}_A$ is of strength $\kappa_1^+ = -\kappa$ and is at $Z_1^{v+} = Z^A + a^2/\overline{(Z_0^{v+} - Z^A)}$, and the image in $\mathscr{C}_B$ is of strength $\kappa_2^+ = -\kappa$ and is at $Z_2^{v+} = Z^B + a^2/\overline{(Z_0^{v+} - Z^B)}$. The successive images are

$$\begin{cases} \kappa_j^+ = (-1)(j+1)/2\kappa, & Z_j^{v+} = Z^A + a^2/\overline{(Z_{j-1}^{v+} - Z^A)} \quad \text{for } j = 3, 5, 7, \ldots \text{ in } \mathscr{C}_A, \\ \kappa_j^+ = (-1)^{j/2}\,\kappa, & Z_j^{v+} = Z^B + a^2/\overline{(Z_{j-3}^{v+} - Z^B)} \quad \text{for } j = 4, 6, 8, \ldots \text{ in } \mathscr{C}_B. \end{cases} \tag{4.3}$$

The other image system, $w_{int}^{v-}$, can be constructed similarly for the top vortex.

Via superposition, the total complex potential is found to be

$$w(Z) = \sum_{j=0}^{N_d} \left( \frac{U_A \mu_j}{Z - Z_j^{dA}} + \frac{U_B \mu_j}{Z - Z_j^{dB}} \right) + \mathrm{i}\kappa \ln(Z - Z_o^{v+}) - \mathrm{i}\kappa \ln(Z - Z_o^{v-}) + \sum_{j=1}^{N_v} [\mathrm{i}\kappa_j^+ \ln(Z - Z_j^{v+}) + \mathrm{i}\kappa_j^- \ln(Z - Z_j^{v-})], \tag{4.4}$$

where $\kappa_j^- = -\kappa_j^+$ and $Z_j^{v-} = \overline{Z_j^{v+}}$ due to symmetry. The infinite dipole and vortex image systems are truncated at the $N_d$ and $N_v$ terms for computation. This potential function is employed to generate the streamlines when two unit cylinders $\mathscr{C}_A$

https://doi.org/10.1017/jfm.2012.45 Published online by Cambridge University Press

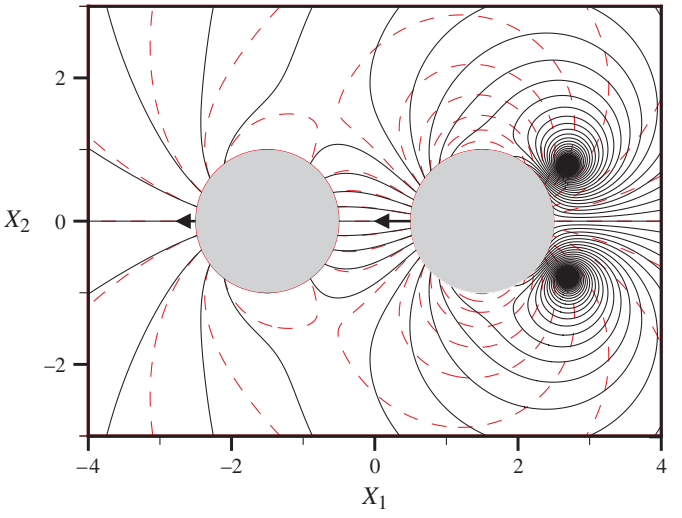



FIGURE 6. (Colour online) The instantaneous streamlines for a system that consists of a cylinder at $(1.5, 0)$ moving at unit velocity towards $-X_1$ with two vortices of $\kappa = \pm 1$ at $(D, H) = (1.2, \mp 0.8)$. The other cylinder moves at half speed from $(-1.5, 0)$ to the left. The interval between each streamline is 0.1.

and $\mathscr{C}_B$ move at $U_A = -1$ and $U_B = -0.5$ from $Z^A = 1.5$ and $Z^B = -1.5$. Using $N_d = 50$, $N_v = 0$ and $\kappa = 0$, the flow streamlines are depicted by the dashed lines in figure 6. When a vortex pair of unit strength is introduced at $(D, H) = (1.2, \mp 0.8)$ from $Z^A$, we used $N_d = N_v = 50$ and $\kappa = 1$ to generate a new flow as shown by the solid lines. It is observed that the streamlines are deflected due to the presence of the vortex pair, suggesting different hydrodynamic forces.

Substituting the *instantaneous* cylinder velocities and locations and the vortex configurations into (4.1)–(4.3), the force on $\mathscr{C}_A$ can be found from (2.9) as

$$F_A = -\frac{\mathrm{d}}{\mathrm{d}t}(AU_A + A^*U_B) + \mathrm{i}2\pi\rho\frac{\mathrm{d}}{\mathrm{d}t}\sum_{\substack{j=1\\ odd\ j}}^{N_v}(\kappa_j^+ Z_j^{v+} + \kappa_j^- Z_j^{v-})$$
$$-2\pi\rho\left[\sum_{\substack{j=0\\ even\ j}}^{N_d}\left(U_A\mu_j\left.\frac{\mathrm{d}f}{\mathrm{d}Z}\right|_{Z_j^{dA}}\right) + \sum_{\substack{j=1\\ odd\ j}}^{N_d}\left(U_B\mu_j\left.\frac{\mathrm{d}f}{\mathrm{d}Z}\right|_{Z_j^{dB}}\right) - \mathrm{i}\sum_{\substack{j=1\\ odd\ j}}^{N_v}(\kappa_j^+ f|_{Z_j^{v+}} + \kappa_j^- f|_{Z_j^{v-}})\right], \quad (4.5)$$

where $A = A_{11} = A_{22} = -\rho\pi a^2 + 2\pi\rho(\mu_0 + \mu_2 + \cdots)$ includes the primary and the image dipoles in $\mathscr{C}_A$. Similarly, $A^* = 2\pi\rho(\mu_1 + \mu_3 + \cdots)$ sums the images in $\mathscr{C}_A$ generated in relation to the motion of $\mathscr{C}_B$. According to (4.1), both $A$ and $A^*$ vary with the inter-cylinder distance, $c$. The partial velocity function, $f$, is composed of all the singularities exterior to $\mathscr{C}_A$ as

$$f(Z) = \sum_{\substack{j=1\\ odd\ j}}^{N_d}\frac{U_A\mu_j}{(Z - Z_j^{dA})^2} + \sum_{\substack{j=0\\ even\ j}}^{N_d}\frac{U_B\mu_j}{(Z - Z_j^{dB})^2} - \frac{\mathrm{i}\kappa}{Z - Z_0^{v+}} + \frac{\mathrm{i}\kappa}{Z - Z_0^{v-}}$$

https://doi.org/10.1017/jfm.2012.45 Published online by Cambridge University Press

| $N_d, N_v$ | $\lvert F_A - F_{A200}\rvert$ | $\lvert F_B - F_{B200}\rvert$ |
|---|---|---|
| 3 | 0.014 | 0.026 |
| 10 | $3.060 \times 10^{-3}$ | $3.990 \times 10^{-4}$ |
| 50 | $3.403 \times 10^{-5}$ | $3.823 \times 10^{-5}$ |
| 100 | $2.798 \times 10^{-7}$ | $3.567 \times 10^{-7}$ |
| 150 | $1.572 \times 10^{-9}$ | $1.803 \times 10^{-9}$ |

TABLE 1. The convergence test for truncating the infinite series in (4.5) and the corresponding force formula for $\mathscr{C}_B$.

$$- \sum_{\substack{j=2 \\ even\ j}}^{N_v} \left( \frac{\mathrm{i}\kappa_j^+}{Z - Z_j^{v+}} + \frac{\mathrm{i}\kappa_j^-}{Z - Z_j^{v-}} \right), \tag{4.6}$$

and is identical for the various terms in (4.5) for the same reason that identical $f$ is adopted in (3.2).

Since the infinite series converge slowly when $c$ approaches 2, a convergence test was performed by checking $F_A$ and $F_B$ at $c = 2.01$ with various $N_d$ and $N_v$ using $U_A = U_B = -1$, $\kappa = 1$ and $(D, H) = (1.2, \mp 0.8)$. The forces computed with $N_d = N_v = 3,\ 10,\ 50,\ 100$ and 150 were compared to the results using 200 terms, denoted by $F_{A200}$ and $F_{B200}$, and the corresponding differences are summarized in table 1. The 50-term partial sum seems to provide a reasonable approximation, with deviation around $O(10^{-5})$, and thus all the infinite series in the following computations are truncated at $N_d = N_v = 50$.

### 4.2. *Validation: constant approach towards a fixed target without the vortex pair*

The set of equations (4.1)–(4.5) is first applied to the literature problem where $\mathscr{C}_A$ is made to move at constant unit velocity towards a fixed $\mathscr{C}_B$ without any vortex for validation. The force on each cylinder can be found using $U_A = -1$ and $U_B = \kappa = 0$ and is scaled by $\rho U_A^2 a$ to calculate the so-called *force coefficient*, $C_d$. Figure 7 shows the results as a function of dimensionless time, $t^* = |U_A|(t - t_0)/a$, with $t_0$ being the time when the two cylinders exactly touch ($c = 2$). On the same plot, the results obtained by Landweber & Shahshahan (1991), Wang (2004) and Bampalas & Graham (2008) are also provided, showing good agreement, except for Wang's data for the moving cylinder at small $t^*$. The deviation may be attributed to the omission of the convection term, $\boldsymbol{v} \cdot \boldsymbol{\nabla}\phi$, in the extended Blasius theorem. Nonetheless, all the works find a dramatic rise of $C_d$ on both cylinders as $\mathscr{C}_A$ moves into the vicinity of $\mathscr{C}_B$.

### 4.3. *Application: a moving Föppl system approaching another cylinder*

In this final section, the derived equations are applied to a problem with two cylinders and a vortex pair. We choose to study how a downstream $\mathscr{C}_B$ may disturb or interact with a moving Föppl system that approaches from far away. Thus, the approaching cylinder, $\mathscr{C}_A$, is made to move at $U_A = -1$ from $c = 30$ with a vortex pair assigned to a centre or saddle equilibrium configuration. We consult the previously studied moving Föppl system to assign the vortex pair, assuming that $\mathscr{C}_B$ has negligible perturbation on its equilibrium at this separation. Using two initial vortex spans $H_0 = 0.25$ and 0.5, two moving Föppl centre equilibrium configurations could be generated with specific $D_0$ and $\kappa$, as provided in table 2. They will be denoted by CI and CII, respectively. Similarly, another three vortex configurations in the moving Föppl saddle equilibrium,

https://doi.org/10.1017/jfm.2012.45 Published online by Cambridge University Press

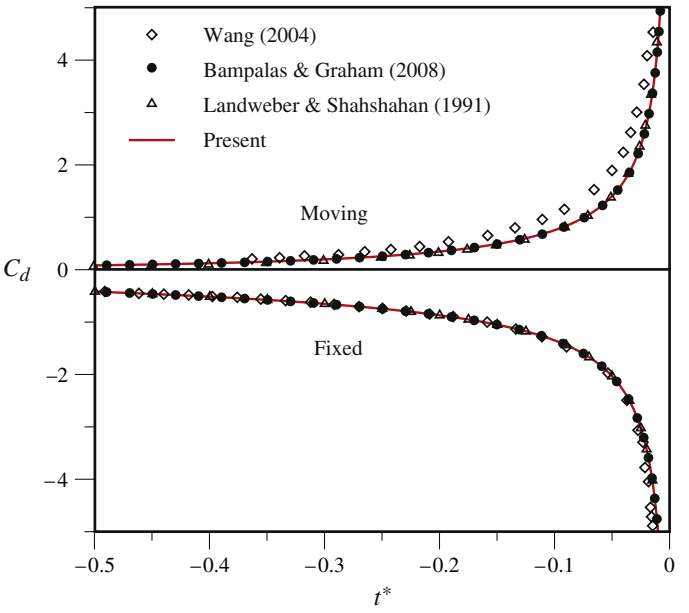



FIGURE 7. (Colour online) Comparison of the force coefficient, $C_d$, on each cylinder as a function of dimensionless time, $t^*$, when $\mathscr{C}_A$ moves normally towards a fixed $\mathscr{C}_B$ at $U_A = -1$ without any vortex.

| Type | $\kappa$ | $H_0$ | $D_0$ |
|---|---|---|---|
| CI | 0.314 187 | 0.25 | 1.256 140 |
| CII | 0.854 102 | 0.5 | 1.538 842 |
| SI | 1.941 125 | 1.0 | 2.197 368 |
| SII | 2.974 788 | 1.5 | 2.942 504 |
| SIII | 3.987 578 | 2.0 | 3.734 203 |

TABLE 2. The strength and the structure required for the vortex pair to remain in a moving Föppl centre or saddle equilibrium, labelled with C or S, respectively.

SI–SIII, are created using larger $H_0 = 1.0$, 1.5 and 2.0 and the corresponding $D_0$ and $\kappa$. The target cylinder is then introduced at a separation of $c = 30$, for which additional image systems are required to ensure the no-penetration boundary conditions on both cylinder surfaces. The newly introduced cylinder does produce additional flow velocity for the five vortex pairs but of a minute magnitude around $O(10^{-5})$ and this perturbation on the moving Föppl equilibrium is assumed to be negligible. The force coefficients on both cylinders are now distinguished by $C_{dA}$ and $C_{dB}$ and examined as a function of $c$ for a fixed or a free $\mathscr{C}_B$.

4.3.1. *Towards a fixed cylinder*

We first examine the case when $\mathscr{C}_B$ is fixed. The force coefficients are depicted on a logarithmic scale in figure 8 for various vortex pair initial configurations. A plus or a minus sign is added to indicate whether the force is positive or negative (noting that $U_A = -1$). The evolution profiles without the free vortex pair are also plotted by the open circles to elucidate the influence of the vortex pair. When the

https://doi.org/10.1017/jfm.2012.45 Published online by Cambridge University Press

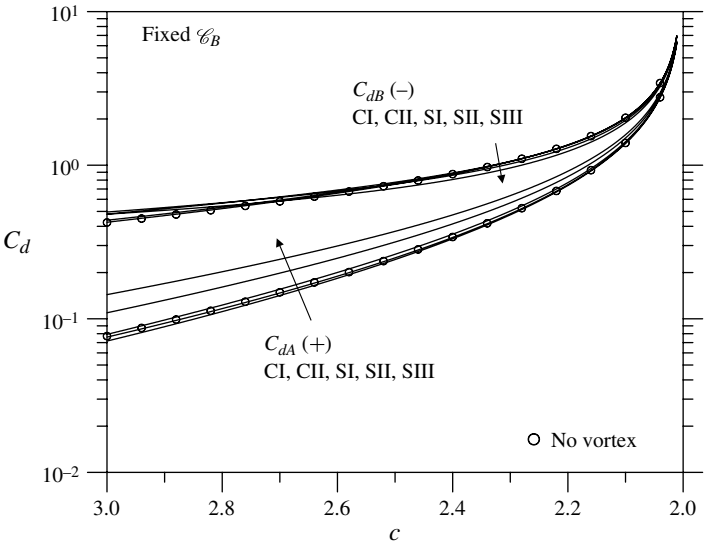



FIGURE 8. Comparisons of the force coefficient on each cylinder, $C_{dA}$ and $C_{dB}$, as a function of the cylinder separation $c$ when $\mathscr{C}_A$ is made to move towards a fixed $\mathscr{C}_B$ at $U_A = -1$ with a vortex pair in different moving Föppl equilibrium configurations summarized in table 2. The open circles show the data when no vortex is present.

vortex pair is initially at the Föppl centre (CI and CII), the force coefficients of both cylinders evolve with $c$ in a manner very similar to that developed without vortices. However, when starting in the Föppl saddle equilibrium (SI–SIII), the vortex pair has negligible influence on the fixed $C_{dB}$ but a greater $C_{dA}$ is observed at the same $c$ with an increment that grows with the vortex structure measured by its $H_0$ or, equivalently, its $D_0$. Possible reasons for these findings will be discussed shortly.

4.3.2. *Towards a free cylinder*

Next, the downstream target $\mathscr{C}_B$ is released and its dynamics is now updated by its equation of motion, $\mathrm{d}U_B/\mathrm{d}t = F_B/(\gamma m_d)$, at each time step. In the present study, we only consider neutrally buoyant $\mathscr{C}_B$ and thus $\gamma = 1$. The cylinder separation–time profiles for all the cases with or without a vortex pair are plotted in figure 9(*a*) by the solid lines. The dashed straight line shows the case with a fixed $\mathscr{C}_B$ and the concave deviation from it indicates a negative displacement of $\mathscr{C}_B$ and an elapsed time longer than $t = 28$ for the two cylinders to contact. Such target cylinder motion is a direct consequence of the pressure field developed around $\mathscr{C}_B$ providing sufficient impulse to set $\mathscr{C}_B$ into motion.

The approach of a moving Föppl system in either initial centre equilibrium configuration results in a $\mathscr{C}_B$ motion nearly identical to that developed without the vortex pair. Thus, the target motion should result primarily from the approach of $\mathscr{C}_A$ and noticeable growth of $U_B$ is observed only at small separation. In these three cases (no vortex, CI and CII), $U_B$ grows from zero to $-0.05$ when $c$ drops to 4.41, 4.47 and 4.87, but $U_B$ speeds up to $-0.26$, $-0.26$ and $-0.28$ at $c = 2.01$. The slight deviation between these cylinder motions can be illustrated better when $U_B$ is presented as a function of $c$ in figure 9(*b*) and the inset therein. The inclusion of a vortex pair in the centre equilibrium helps to set $\mathscr{C}_B$ into faster motion than induced by only an approaching $\mathscr{C}_A$, but at a degree detectable only when the pair is in the CII condition.

https://doi.org/10.1017/jfm.2012.45 Published online by Cambridge University Press

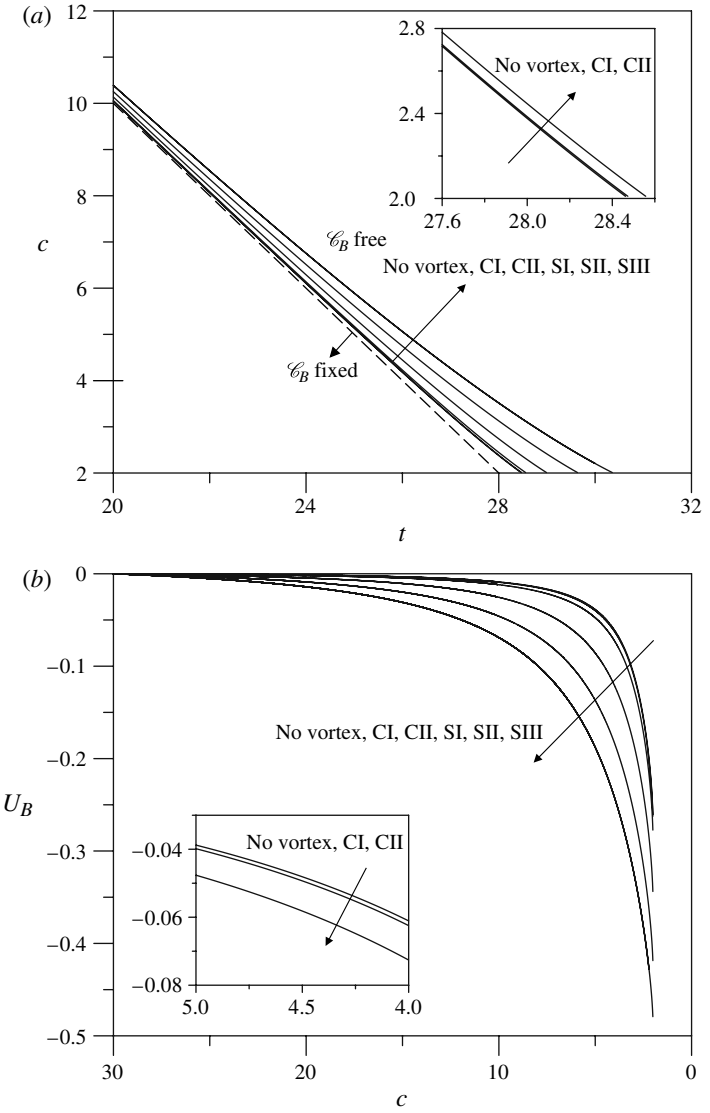



FIGURE 9. Comparison of the target cylinder evolution dynamics in different cases: (*a*) the cylinder separation $c$ as a function of time $t$; (*b*) $U_B$ as a function of $c$.

In contrast, when the vortex pair forms a moving Föppl saddle equilibrium with $\mathscr{C}_A$, their approach sets the target into apparent motion at much larger separation, as shown in figure 9(*b*), corresponding to a greater deviation of their $c$–$t$ curves from the straight dashed line in figure 9(*a*). The degree of induced motion again grows with the strength and the structure size of the vortex pair. For example, the time for contact with the vortex pair in SI, SII and SIII configurations increases slightly from 28.99 to 29.63 and 30.35. The respective target velocity grows to $U_B = -0.05$ at $c = 6.93$, 9.55 and 11.94 and reaches its peak of $-0.34$, $-0.42$ and $-0.48$ at $c = 2.01$. These values are to be compared with the values measured when $\mathscr{C}_B$ is fixed. Such a positive correlation between the induced target motion and the vortex strength and structure is attributed to the fact that the greater fluid impulse carried by a stronger and larger vortex pair can

https://doi.org/10.1017/jfm.2012.45 Published online by Cambridge University Press

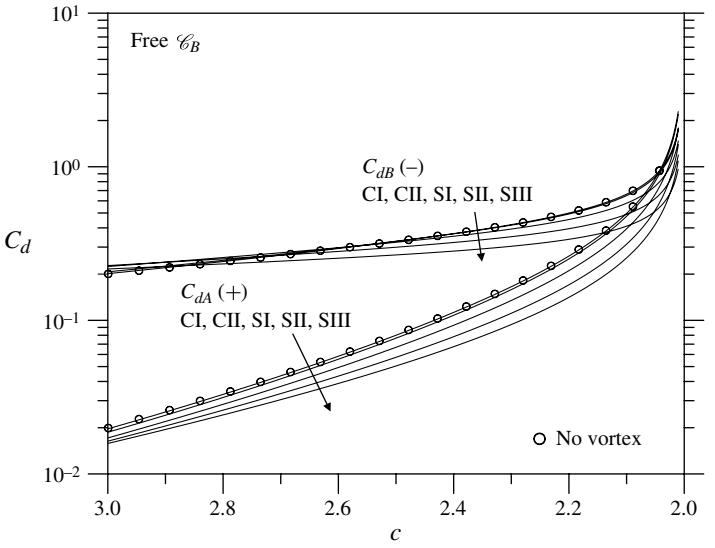



FIGURE 10. Comparisons of the force coefficient on each cylinder, $C_{dA}$ and $C_{dB}$, as a function of $c$ when a moving Föppl system moves towards a free $\mathscr{C}_B$ in different equilibrium configurations. The open circles show the data when no vortex is present.

modify the flow around $\mathscr{C}_B$ more effectively. Such force augmentation with the vortex structure can also be inferred from figure 9 in Shashikanth (2006), where the object acceleration is examined.

When the force coefficients on both cylinders are examined as a function of $c$ in figure 10, a monotonic increase of both $C_{dA}$ and $C_{dB}$ with diminishing $c$ is observed but at a *lower* rate in comparison to how they develop with a fixed $\mathscr{C}_B$. For both cylinders, the force evolutions in the cases of CI, CII and that without the vortex pair show nearly identical profiles, suggesting that the flow induced by a constantly moving $\mathscr{C}_A$ is not altered much by these two vortex pairs. The mobility of $\mathscr{C}_B$, however, degrades the hydrodynamic force: the peak $C_{dA}$ and $C_{dB}$ at $c = 2.01$ is only 37 and 26 % or so of the corresponding values with $\mathscr{C}_B$ being fixed.

The force deduction is even more pronounced when the vortex pair approaches in moving Föppl saddle equilibrium, with a growing degree from SI to SIII configurations. The peak $C_{dA}$ developed at $c = 2.01$ for the SI–SIII cases now drops to 28, 22 and 17 % of that measured with a stationary target. A more severe magnitude degradation is found for $C_{dB}$ to even lower percentage: 21, 17 and 14 %. However, by comparing the force deduction percentages resulting from the mobility of $\mathscr{C}_B$ and from the inclusion of a vortex pair, it can be concluded that the former has a stronger influence on the total force coefficients. The effect of a vortex pair is only secondary, at least for the currently studied cases, owing to its originally weak strength.

In addition to the force degradation, two distinctive features are observed in the current $C_d$–separation profiles for a moving target. Firstly, at the same separation, a smaller $C_{dA}$ is developed with a larger and stronger vortex pair in figure 10, which contrasts with the correlation for $C_{dA}$ illustrated in figure 8 when $\mathscr{C}_B$ is fixed. Secondly, the moving target now experiences different $C_{dB}$ at small separation in the SI–SIII cases, which is to be compared to the conforming profiles measured on a fixed $\mathscr{C}_B$

https://doi.org/10.1017/jfm.2012.45 Published online by Cambridge University Press

in figure 8. All these phenomena result from a combined effect of a smaller relative motion between $\mathscr{C}_A$ and $\mathscr{C}_B$ and a negative $U_B$, as explained below.

Recall that it has been concluded that the mobility of $\mathscr{C}_B$ has a stronger influence on the system dynamics than the vortex pair configuration. It is thus speculated that the total force evolution can be characterized by the first term on the right-hand side of (4.5), $-\mathrm{d}(AU_A + A^*U_B)/\mathrm{d}t$, which generates the time rate change of fluid impulse due to variations in the cylinder relative configuration. With the chain rule, $\mathrm{d}/\mathrm{d}t = (U_A - U_B)\,\mathrm{d}/\mathrm{d}c$, this force component can be expressed as

$$-\frac{\mathrm{d}}{\mathrm{d}t}(AU_A + A^*U_B) = -U_A(U_A - U_B)\frac{\mathrm{d}A}{\mathrm{d}c} - U_B(U_A - U_B)\frac{\mathrm{d}A^*}{\mathrm{d}c} - A^*\frac{\mathrm{d}U_B}{\mathrm{d}t}. \quad (4.7)$$

By definition, $A$ is positive but $A^*$ is negative, and their spatial derivatives with respect to $c$ give $\mathrm{d}A/\mathrm{d}c < 0$ and $\mathrm{d}A^*/\mathrm{d}c > 0$. Thus, when $U_B = 0$, (4.7) is reduced to $-U_A^2\,\mathrm{d}A/\mathrm{d}c$, giving a positive contribution to $F_A$, as opposed to $U_A = -1$ as revealed in figure 8. When $\mathscr{C}_B$ is set into a negative motion, this positive term diminishes for $|U_A - U_B| < |U_A|$. Further, with $|U_A| > |U_B|$ for the current cases, the second term in (4.7) is negative, which acts with the last negative term to further degrade the total hindering $F_A$. At the same separation, such diminishing effect is more pronounced when the vortex pair strength and structure are greater, since the induced $U_B$ is larger (see figure 9*b*). Thus, the SIII case results in the lowest $C_{dA}$ in figure 10. It is also the deviation in the target cylinder motion that renders deviating $C_{dB}$ evolution profiles in that particular ordering.

Lastly, it is noted that $C_{dB}$ always exceeds $C_{dA}$, and the difference is larger when $\mathscr{C}_B$ is free to move. This phenomenon is explained here by the behaviour of the first two components in (4.7) that dominate the total hydrodynamic force on both cylinders. When $\mathscr{C}_B$ is fixed, this component contributes $-U_A^2\,\mathrm{d}A/\mathrm{d}c$ to $F_A$ and $-U_A^2\,\mathrm{d}A^*/\mathrm{d}c$ to $F_B$, and it is the fact that $|\mathrm{d}A^*/\mathrm{d}c| > |\mathrm{d}A/\mathrm{d}c|$ when $c > 2.0$ that renders $|F_B| > |F_A|$. According to the definition of $A$ and $A^*$, the largest components in $\mathrm{d}A^*/\mathrm{d}c$ and $\mathrm{d}A/\mathrm{d}c$ are $\mathrm{d}\mu_1/\mathrm{d}c$ and $\mathrm{d}\mu_2/\mathrm{d}c$, respectively. The fact that the consecutive image dipole strength decays rapidly with increasing separation suggests a much greater $|\mathrm{d}A^*/\mathrm{d}c|$ than $|\mathrm{d}A/\mathrm{d}c|$ at large $c$ and hence we observe $|F_B| > |F_A|$ in figure 8. Now, the opposite occurs for the forces induced by a non-zero $U_B$, since the image system generated in $\mathscr{C}_A$ now depends on $\mathrm{d}\mu_1/\mathrm{d}c$ and the consecutive terms with odd indices and their sum would exceed that formed in $\mathscr{C}_A$. The two image dipole systems generated for $U_A$ and $U_B$ would compensate each other since the two cylinders move in the same direction. Thus, for $\mathscr{C}_A$, the smaller force due to the weaker $U_A$-induced image system is now counteracted by a stronger $U_B$-induced image system; the force from the stronger $U_A$-induced image system in $\mathscr{C}_B$ is only reduced by a smaller amount due to the weaker $U_B$-induced image system. Consequently, a larger deviation between $C_{dA}$ and $C_{dB}$ is observed in figure 10 with a free $\mathscr{C}_B$ than that revealed in figure 8.

## 5. Conclusions and remarks

In this work, the two-dimensional Lagally theorem that describes the hydrodynamic force on a solid object moving in an inviscid and incompressible fluid has been extended successfully to include free vortices. An explicit force formula has been derived in terms of the properties of the singularities employed to create the motion of the body and the ambient flow structure and to ensure the no-penetrating boundary condition. One advantage of the current force formula is that it requires only algebraic

https://doi.org/10.1017/jfm.2012.45 Published online by Cambridge University Press

manipulation, provided that the object shape and its boundary condition can be handled with the potential flow theory. Nonetheless, the true merit is appreciated in a multi-body problem where the individual force can be obtained using the respective internal singularities, a task that falls beyond the scope of the conventional Lagally theorem, which gives the lumped sum of the forces on all the surfaces.

The newly developed force formula (2.9) is validated by reproducing the equation of motion and the dynamics of three flow–body interaction problems in the literature. The first examines the relative trajectory between a cylinder when interacting with a free vortex. The second problem deals with the moving Föppl problem, and the derived equations of motion for both the cylinder and the vortex pair are employed for an extended bifurcation analysis on the system dynamics. In the third case, a cylinder is forced to move normally towards a fixed identical target and the hydrodynamic force developed on each cylinder is calculated using the current force formula. The results are in good agreement with the literature works, which use either the Lagrangian mechanics in conjunction with the generalized Taylor theorem or the extended Blasius theorem.

We then extended the problem to introduce a vortex pair behind the approaching cylinder using the equilibrium configurations determined for a moving Föppl system, provided that the perturbation from the far-downstream target is negligible. The force developed on each cylinder is studied with respect to the vortex pair structure and compared to that found without any free vortex. A greater force is measured when the vortex pair has stronger circulation and larger structure, but such augmentation is more pronounced when the vortex pair is initially in moving Föppl saddle equilibrium. Finally, when the target cylinder is allowed to move, its mobility greatly modifies the hydrodynamic force by reducing its magnitude and reversing the force ordering with respect to vortex pair structures.

We would like to report that, for all the cases examined in this work, the vortex pair structure remains nearly unchanged throughout the approach, regardless of the target mobility. The maximum deviation in either $H$ or $D$ never exceeds 1 % from its initial equilibrium values, $H_0$ or $D_0$, which may explain why we observed a stronger influence of target mobility on the drag coefficients than vortex pair structure. Such robustness in vortex pair structure under the perturbation from a downstream target may be correlated to how the system total impulse is distributed on the solid and the fluid phases, an aspect that should provide other information for a fully coupled fluid–body interaction problem and will be pursued in future studies.

Undoubtedly, richer dynamics for this system of two cylinders and one vortex pair can be generated by using arbitrary vortex strength and configuration and changing the target cylinder density. The problem when $\mathscr{C}_A$ is no longer in forced motion is also worth a thorough investigation. It is of great interest to extend the current theorem to incorporate changes in object volume by time-varying sources, to generate lift on the object by an internal vortex, and to handle irregular object shapes. This latter task has been considered by Kanso & Oskouei (2008) using the technique of conformal mapping to study the interaction of an ellipse with vortex pairs.

## REFERENCES

BAMPALAS, N. & GRAHAM, J. M. R. 2008 Flow-induced forces arising during the impact of two circular cylinders. *J. Fluid Mech.* **616**, 205–234.

BIESHEUVEL, A. 1985 A note on the generalized Lagally theorem. *J. Engng Maths* **19**, 69–77.

BIRKHOFF, G. 1950 *Hydrodynamics*. Princeton University Press.

https://doi.org/10.1017/jfm.2012.45 Published online by Cambridge University Press

BORISOV, A. V., MAMAEV, I. S. & RAMODANOV, S. M. 2003 Motion of a circular cylinder and $n$ point vortices in a perfect fluid. *Regular Chaotic Dyn.* **8**, 449–462.

CROWDY, D. G. 2008 Explicit solution for the potential flow due to an assembly of stirrers in an inviscid fluid. *J. Engng Maths* **62**, 333–344.

CROWDY, D. G. 2010 A new calculus for two-dimensional vortex dynamics. *Theor. Comput. Fluid Dyn.* **24**, 9–24.

CROWDY, D. G. & MARSHALL, J. S. 2005*a* Analytical formulae for the Kirchhof–Routh path function in multiply connected domains. *Proc. R. Soc. Lond.* A **461**, 2477–2501.

CROWDY, D. G. & MARSHALL, J. S. 2005*b* The motion of a point vortex around multiple circular islands. *Phys. Fluids* **17**, 056602.

CUMMINS, W. E. 1953 The forces and moments acting on a body moving in an arbitrary potential stream. *David Taylor Model Basin, Rep. no.* 708.

EAMES, I., LANDERYOU, M. & FLÓR, J. B. 2007 Inviscid coupling between point symmetric bodies and singular distributions of vorticity. *J. Fluid Mech.* **589**, 33–56.

FÖPPL, L. 1913 Wirbelbewegung hinter einem Kreiszylinder. *Sitz. K. Bäyr. Akad. Wiss.* **1**, 7–18.

KANSO, E. & OSKOUEI, B. G. 2008 Stability of a coupled body–vortex system. *J. Fluid Mech.* **600**, 77–94.

LAGALLY, M. 1922 Berechnung der Kräfte und Momente, die strömende Flüssigkeiten auf ihre Begrenzung ausüben. *Z. Angew. Math. Mech.* **2**, 409–422.

LAMB, H. 1932 *Hydrodynamics*. Dover.

LANDWEBER, L. 1956 On a generalization of Taylor's virtual mass relation for Rankine bodies. *Q. Appl. Maths* **14**, 51–56.

LANDWEBER, L. & CHWANG, A. T. 1989 Generalization of Taylor's added-mass formula for two bodies. *J. Ship Res.* **33**, 1–9.

LANDWEBER, L. & MILOH, T. 1980 Unsteady Lagally theorem for multipoles and deformable bodies. *J. Fluid Mech.* **96**, 33–46.

LANDWEBER, L. & SHAHSHAHAN, A. 1991 Added masses and forces on two bodies approaching central impact in an inviscid fluid. *Tech. Rep.* 346. Iowa Institute of Hydraulic Research.

LANDWEBER, L. & YIH, C.-S. 1956 Forces, moments, and added masses for Rankine bodies. *J. Fluid Mech.* **1**, 319–336.

MARSHALL, J. S. 2001 *Inviscid Incompressible Flow*. Wiley-Interscience.

MILNE-THOMPSON, L. M. 1968 *Theoretical Hydrodynamics*. Dover.

SAFFMAN, P. G. 1992 *Vortex Dynamics*. Cambridge University Press.

SEDOV, L. I. 1965 *Two-Dimensional Problems in Hydrodynamics and Aerodynamics*. John Wiley & Sons.

SHASHIKANTH, B. N. 2006 Symmetric pairs of point vortices interacting with a neutrally buoyant two-dimensional circular cylinder. *Phys. Fluids* **18**, 127103.

SHASHIKANTH, B. N., MARSDEN, J. E., BURDICK, J. W. & KELLY, S. D. 2002 The Hamiltonian structure of a two-dimensional rigid circular cylinder interacting dynamically with $N$ point vortices. *Phys. Fluids* **14**, 1214–1227.

TAYLOR, G. I. 1928 The energy of a body moving in an infinite fluid, with an application to airships. *Proc. R. Soc. Lond.* A **120**, 13–21.

TCHIEU, A. A., CROWDY, D. & LEONARD, A. 2010 Fluid–structure interaction of two bodies in an inviscid fluid. *Phys. Fluids* **22**, 107101.

WANG, Q. X. 2004 Interaction of two circular cylinders in inviscid fluid. *Phys. Fluids* **16**, 4412–4425.

YANG, F.-L. 2010 A formula for the wall-amplified added mass coefficient for a solid sphere in normal approach to a wall and its application for such motion at low Reynolds number. *Phys. Fluids* **22**, 123303.

https://doi.org/10.1017/jfm.2012.45 Published online by Cambridge University Press